Journal of Materials Chemistry C

Accepted Manuscript

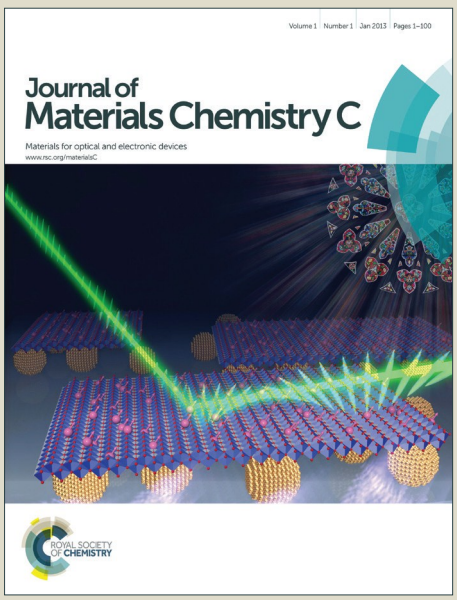

ROYAL SOCIETY OF CHEMISTRY

www.rsc.org/materialsC

Journal of Materials Chemistry C

Dielectric investigation on high-k Yttrium Copper Titanate thin films

Anna Grazia Monteduro[a, b], Zoobia Ameer[a, b], Maurizio Martino[a], Anna Paola Caricato[a], Vittorianna Tasco[b], Indira Chaitanya Lekshmi[c, ◊], Ross Rinaldi[a, c], Abhijit Hazarika[d], Debraj Choudhury[d, e], D. D. Sarma[d, f, *], Giuseppe Maruccio[a, b, *]

Received 00th January 20xx,
Accepted 00th January 20xx

DOI: 10.1039/x0xx00000x

www.rsc.org/

We report on the first dielectric investigation of high-k Yttrium Copper Titanate thin films, which demonstrated to be very promising for nanoelectronics applications. The dielectric constant of these films is found to vary from 100 down to 24 (at 100 kHz) as a function of deposition conditions, namely oxygen pressure and film thickness. The physical origin of such variation was investigated in the framework of universal dielectric response and Cole-Cole relations and by means of voltage dependence studies of the dielectric constant. Surface-related effects and charge hopping polarization processes, strictly dependent on the film microstructure, are suggested as the main responsible of the observed dielectric response. In particular, the bulky behaviour of thick films deposited at lower oxygen pressure evolves towards a more complex and electrically heterogeneous structure when either the thickness decreases down to 50 nm or the films are grown under high oxygen pressure.

Introduction

Rare earth copper titanates of the Ln_2CuTiO_6 family are promising high-k materials with an unusual combination of advantageous dielectric properties, such as low dielectric loss and weak temperature and frequency dependences, beyond the high dielectric constant[1-3]. Structural studies[4-7] demonstrated that Ln_2CuTiO_6 compounds have (i) the structure isotypical to $LnMnO_3$ manganites, exhibiting an orthorhombic to hexagonal structural transition as a function of the *Ln* rare earth size; (ii) a non-centrosymmetric crystal structure (the hexagonal compounds only), (iii) two transition metal ions randomly distributed among the B sites and having a different mixed valence character, namely Cu(I)/(II) and Ti(III)/(IV), which is due to oxygen-vacancies.

As far as the dielectric properties are concerned, a number of hexagonal (*Ln*=Y, Yb, Er, Ho, Dy) and orthorhombic (*Ln*=La, Pr, Nd) Ln_2CuTiO_6 compounds have been recently investigated in bulk form[1-3], revealing a higher frequency and temperature stability of the dielectric constants and lower dielectric losses for the first family. In particular, Choudhury et al.[8] reported that Ho_2CuTiO_6 (HCTO) exhibits a nearly stable dielectric constant of 53 (from 10 K to 450 K and from 100 Hz to 1 MHz) and suggested that the random distribution of the different transition metal ions over the B sites combined with the very different sizes for Cu/Ti trigonal bipyramids could be responsible for both the ferroelectricity frustration and the unusually stable dielectric properties. Yang et al.[9] investigated strong dielectric relaxations in La_2CuTiO_6 (LCTO) ceramics, and found a correlation between the giant dielectric constant with the mixed valence character induced by oxygen vacancies. The similar mixed valence structure has been observed also in $CaCu_3Ti_4O_{12}$ ceramics and it is considered a possible origin of the giant dielectric constant[10, 11].

Despite these promising results, the deposition and dielectric characterization of hexagonal copper titanate thin films have not been investigated so far. In this paper, we report on the first detailed dielectric behaviour study performed on amorphous YCTO thin films, deposited by pulsed laser deposition. Among the (better performing) hexagonal Ln_2CuTiO_6 compounds, we choose Y_2CuTiO_6, which is the cheapest compound of the family but still maintains the desirable properties for device applications: high dielectric constant, low loss and weak frequency and temperature dependencies. Specifically, we investigated the film dielectric response in a wide range of growth parameters, namely the oxygen pressure and the thickness, observing a notable variation on the dielectric constant, from 24 to 100 at an applied frequency of 100 kHz. Accurate dielectric dispersion analysis and voltage dependent

[a] Department of Mathematics and Physics, University Of Salento, Via per Arnesano, 73100, Lecce, Italy.
[b] CNR NANOTEC - Istituto di Nanotecnologia, Via per Arnesano, 73100 Lecce, Italy.
[c] CNR NANO - Istituto Nanoscienze, Via per Arnesano, 73100 Lecce, Italy.
[d] *Solid State and Structural Chemistry Unit, Indian Institute of Science, Bangalore, 560012, India.*
[e] *Department of Physics, Indian Institute of Technology Kharagpur, Kharagpur 721302, India*
[f] *Council of Scientific and Industrial Research - Network of Institutes for Solar Energy (CSIR-NISE), New Delhi, India*
◊ Present address: Dept of Chemistry, CMR Institute of Technology, 132, AECS layout, IT Park Road, Bangalore 560037.

* Corresponding authors: giuseppe.maruccio@unisalento.it, sarma@sscu.iisc.ernet.in

studies allowed to shed light on the physical origin of the dielectric response.

Experimental

The YCTO thin films were deposited by pulsed laser deposition (PLD) with an ArF excimer laser (Lamba Physics 305i, λ=193 nm, τ=20ns) on Si/SiO_2 (500 µm / 5 µm) substrates with lithographed bottom electrodes. The YCTO target was prepared by solid states synthesis as described elsewhere[1] and the ablation process was carried out with an energy density of $2J/cm^2$ and a repetition rate of 10 Hz. The substrates were placed parallel to the target at a distance of 4.5 cm. During deposition the substrate was heated at a temperature of 600°C and the oxygen pressure was varied from 0.05 Pa to 0.5 Pa in different growths, since it is a crucial factor for maintaining oxygen stoichiometry in the films[12, 13]. The number of pulses was also varied in order to study the thickness effect on the dielectric properties of the films with higher permittivity values. After deposition, the films were cooled at a rate of 5°C/min while maintaining the same oxygen pressure. Thickness of YCTO films was evaluated using a surface profilometer (Veeco Dektak 6M). Henceforward, we will use the following notation to refer to the samples: $Y|_{t_i}^{PO_2}$, where the upper index refers to the oxygen pressure value (0.05 Pa or 0.5 Pa) and the lower index, t_i (i=1,2,3), indicates the thickness of the film (t_1=300 nm, t_2=150 nm and t_3=50 nm).

The crystal structure of the films was examined using X-ray diffraction (XRD) (model X'Pert PRO, PANalytical) performed at grazing incident angle (GIXRD) (ω=1°) to maximize film signal by limiting the substrate effect. A Nichel filter was used to cut fluorescence background in these experiments.

The chemical composition was determined by X-ray fluorescence spectroscopy (XRF) using an X-Ray spectrometer (EDAX Orbis) equipped with a rhodium X-ray tube and a Si(Li) Be-Window Detector.

For carrying out the dielectric measurements, a cross-bar architecture was employed (Fig. 1). Parallel Cr (6nm)/Au (60nm) electrodes with lateral sizes ranging from 5 µm to 300 µm were fabricated below and above the YCTO film by standard photolithography and lift-off techniques. For each film, 64 junctions, with different areas ranging from 25 μm^2 to 90000 μm^2, were realized enabling an accurate dielectric analysis.

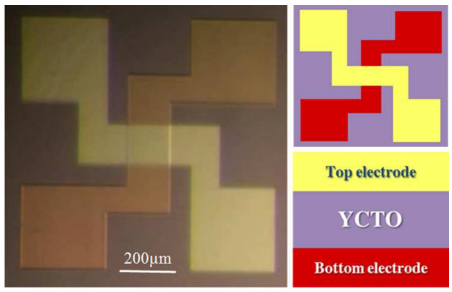

Fig. 1 Optical image of a typical MIM junction and sketches of its top and cross view.

The impedance spectroscopy measurements were performed at room temperature by an Agilent E4980A precision LCR meter over the frequency range from 100 Hz to 1 MHz using an AC-driving voltage (V_{AC} = 100mV). The electrical contacts were performed by using tungsten probes of 40 µm in diameter.

When measuring the dielectric constant of thin films, parasitic capacitances can affect measurements, especially in the case of small junctions. Here, for a more accurate evaluation of the real (ε') and imaginary part (ε'') of complex dielectric permittivity ($\varepsilon^* = \varepsilon' - j\varepsilon''$), respectively the dielectric constant and loss, a parametric study was performed by analysing for each deposited sample a large number (usually 64) of metal-insulator-metal (MIM) capacitors having different junction areas. Since each junction can be considered as a parallel plate capacitor, the expected capacitance is:

$$C = \frac{\varepsilon_0 \varepsilon' S}{d} \quad (1)$$

where ε_0 is the permittivity of free space, ε' is the real part of the complex dielectric permittivity (ε^*) of the material, *S* the area of the junction and *d* the thickness of the film. Any junction contribution to the capacitance is expected to linearly scale with the area, except the contribution of spurious capacitances, which can be related to the circuit. As a consequence, by means of a linear fit of the measured capacitance (*C*) versus junction area (*S*) curve at each frequency, both the dielectric constant and the parasitic capacitance can be extrapolated respectively, from the obtained slope and intercept values. Thus this procedure permits a quantitative comparison of the frequency dependence of the dielectric constant values ($\varepsilon'(\omega)$, where ω=2πf and f the frequency) in the different films.

The imaginary part ($\varepsilon''(\omega)$) of the complex dielectric permittivity was also extracted by means of a fitting procedure over the junction areas. In particular from the measured capacitance and tangent loss (Tgδ), the latter defined as:

$$Tg\delta = \frac{\varepsilon''}{\varepsilon'} \quad (2)$$

we calculated the conductance (G=ωCTgδ). Since G depends on the junction geometry, we extracted the conductivity σ from the slope of the G vs S linear fit at each frequency. Then, $\varepsilon''(\omega)$ was derived by $\sigma(\omega)$, as $\sigma(\omega) = \omega\varepsilon_0\varepsilon''(\omega)$.

To check for interfacial polarization effect, voltage dependence measurements were carried out over-imposing a fixed DC bias (V_{DC}) to the driving AC-voltage in order to measure the permittivity dispersion ($\varepsilon' - f$) in the full frequency range at different DC bias. Moreover, the electric field (E) dependence of the capacitance percentage variation $\left(\frac{\Delta C(V)}{C(0)}(\%) - E, \text{ where } \frac{\Delta C(V)}{C(0)} = \frac{C(V)-C(0)}{C(0)}\right)$ was also evaluated by sweeping the DC-bias from positive to negative values at a fixed AC frequency (1 kHz).

Results and discussion

Structural and chemical composition characterization

In spite of the relatively high substrate temperature (600°C), the films presented an amorphous character as evidenced by the XRD spectra (Fig.2) where no sharp diffraction peaks are visible in contrast to the target spectrum (coloured in gray), showing the typical reflection of a polycrystalline structure characterized by hexagonal unit cell with space group $P6_3cm$, as reported in ref. 2.

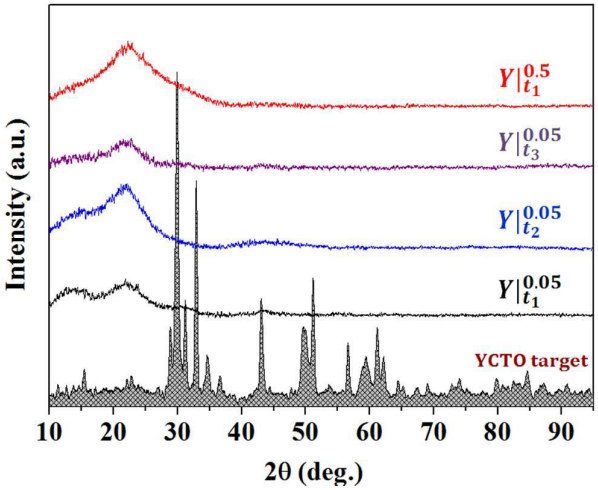

Fig. 2 XRD spectra of the amorphous YCTO thin films deposited by PLD. The XRD scan of the YCTO target is also reported as a reference (grey filled).

In Table 1 we summarized the weight percentage (%Wt), the atomic percentage (%At) and the stoichiometric index of the cations in the different films extracted by XRF. Several areas along the sample surface have been inspected, showing homogeneous composition profile. We observed minor differences within each film (with lateral size of 1x1 cm^2) and from one film to the other, but we found a stoichiometry quite different from the Y_2CuTiO_6 target (green curve). In particular, the spectra in Fig. 3 indicate a deficiency in Yttrium and an excess of Titanium, while Copper appears in the right atomic ratio (and we normalized the spectra on this ion for this reason). We explain this finding as a result of a re-sputtering process during PLD growth which is expected to more strongly affect the heaviest atoms[14]. This change in the stoichiometry could affect the final film structure, facilitating the formation of an amorphous film useful for electronic applications.

Dielectric characterization

Fig. 4 summarizes the frequency dependences of the dielectric constant (ε') and dielectric loss (ε'') for the investigated YCTO films, as a function of their oxygen deposition pressure (P_{O_2}) and thickness. Specifically, we found a relatively high value of dielectric constant (≈100) at 100 kHz for the film deposited at 0.05 Pa ($Y|_{t_1}^{0.05}$) which decreases to 23.6 for $Y|_{t_1}^{0.5}$ grown at a significantly larger oxygen pressure (0.5Pa). This last value approaches the permittivity reported for bulk YCTO (40.3 in ref.1, and 17 in ref.2 at 100 kHz).

These results are interesting from a technological point of view, since they indicate that YCTO exhibits a high dielectric constant also as a thin film, with a wide tunability range driven by the deposition conditions.

However, a key prerequisite for any future application is a better understanding of the physical origin of this high permittivity (especially at low oxygen deposition pressure). In this respect, the first issue we investigated was the evaluation of the non-intrinsic contribution of surface barriers or electrode polarization effects in determining the film dielectric response by means of a thickness dependent study, at a fixed P_{O_2} = 0.05Pa. These mechanisms have been widely reported in several ferroelectric thin films, such as STO[15], BST[16, 17], BNT[18], PZT[19, 20] and high-k dielectric materials, such as $CaCu_3Ti_4O_{12}$[21, 22] showing in all these cases a clear thickness-dependence.

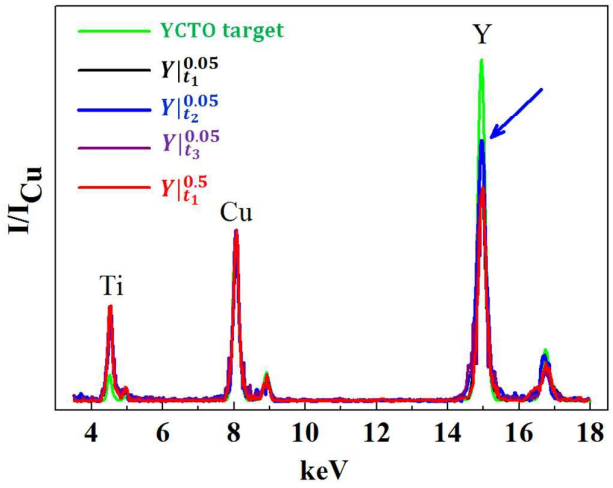

Fig. 3 XRF spectra of the YCTO films and target normalized with respect to the Cu.

Table 1 Summary of the XRF analysis results.

sample	Element	%Wt	%At	St. index
target	Y	63.58	52.15	**2.09**
	Cu	20.24	23.23	**0.93**
	Ti	16.18	24.62	**0.98**
$Y\|_{t_1}^{0.05}$	Y	38.16	26.83	**1.07**
	Cu	23.44	23.06	**0.92**
	Ti	38.40	50.11	**2.00**
$Y\|_{t_2}^{0.05}$	Y	43.03	30.86	**1.23**
	Cu	20.45	20.52	**0.82**
	Ti	36.52	48.62	**1.94**
$Y\|_{t_3}^{0.05}$	Y	37.55	26.28	**1.05**
	Cu	23.15	22.67	**0.91**
	Ti	39.30	51.05	**2.04**
$Y\|_{t_1}^{0.5}$	Y	38.00	26.65	**1.07**
	Cu	22.93	22.50	**0.90**
	Ti	39.07	50.86	**2.03**

To take into account these effects, the measured capacitance (C) can be expressed as the series between interfacial capacitance (C_i) and bulk film capacitance (C_b):

$$\frac{1}{C} = \frac{1}{C_b} + \frac{1}{C_i} \quad (3)$$

which can be written in term of dielectric constant :

$$\frac{d}{\varepsilon'} = \frac{d-2d_i}{\varepsilon'_b} + \frac{2d_i}{\varepsilon'_i} \approx \frac{d}{\varepsilon'_b} + \frac{2d_i}{\varepsilon'_i} \quad (4)$$

where d is the total film thickness, d_i is the interfacial layer thickness, ε'_b is the bulk film dielectric constant, and ε'_i is the interfacial layer dielectric constant, considering dielectrically similar the interfacial layers at both electrodes. Since the interfacial layer is expected to be much thinner than the bulk of the film (d_i<<d), the second term of the previous equation can be approximated as reported above. Therefore a linear relationship is expected between *d/ε'* and *d*.

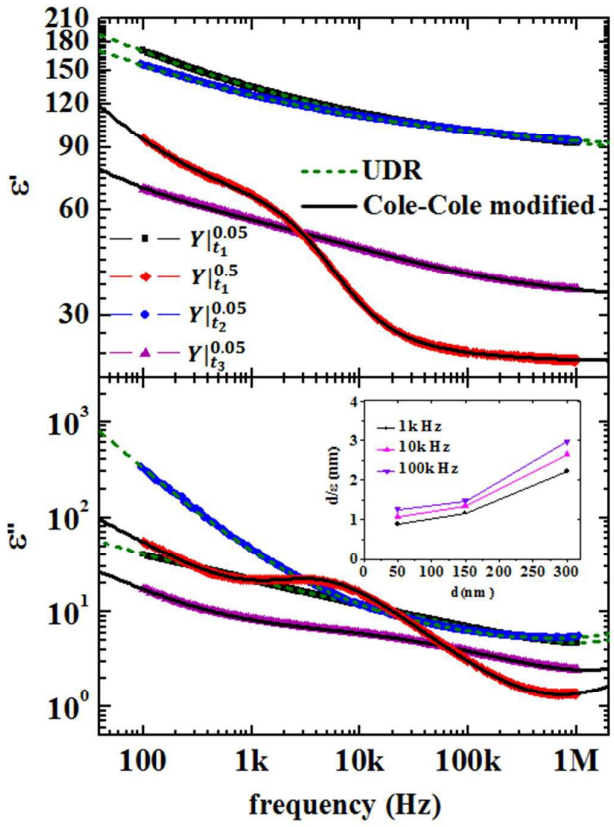

Fig. 4 Frequency dependences of real (ε') and imaginary part (ε'') of the complex permittivity in the frequency range 100 Hz - 1 MHz for all deposited YCTO films. The solid curves are the best fits to modified Cole-Cole equations for ε' and ε''; and the dashed curves are the best fits to universal dielectric response (UDR) equations. Inset: thickness-dependence of the dielectric constant of the film deposited at 0.05 Pa with thickness of 300 nm, 150 nm and 50 nm.

In our study of samples grown at the lowest P_{O_2} ($Y|_{t_i}^{0.05}$), we observed only minor changes of ε'(f) (around 100 at 100 kHz) when the thickness is reduced from 300 nm ($Y|_{t_1}^{0.05}$) to 150 nm ($Y|_{t_2}^{0.05}$), while a further decrease to 50 nm ($Y|_{t_3}^{0.05}$) results in a relevant drop in ε'(≈40). A similar trend was observed also for samples deposited at 0.1Pa (see Fig. S1 in the Supporting Information). However by plotting *d/ε'* versus *d* (Fig. 4 inset) the data deviate from the linearity, suggesting that a unique ε'_b value for all the explored film thicknesses is not a proper assumption. Therefore we supposed that there could be other factors, probably related to the film microstructure, in addition to the electrode/sample interface, affecting the thickness variation of the permittivity in the YCTO thin films.

Further insight in the involved physical mechanisms comes from a closer examination of the dielectric dispersion when comparing $Y|_{t_1}^{0.05}$ and $Y|_{t_1}^{0.5}$ films, which differ not only for the permittivity value, but also in the frequency dependence. As shown in Fig. 4, $Y|_{t_1}^{0.05}$ displays a typical power law frequency dependence behaviour, with both real (ε') and imaginary parts (ε'') of the complex permittivity decreasing with frequency. On the other hand, $Y|_{t_1}^{0.5}$ shows a Debye-like dielectric relaxation with a smeared step in ε' accompanied by a broad peak in ε'' at intermediate frequencies (around 5 kHz). In addition, it should be noted that among the films deposited at 0.05 Pa, $Y|_{t_2}^{0.05}$ behaves as $Y|_{t_1}^{0.05}$, while the response of the thinnest film ($Y|_{t_3}^{0.05}$) reminds that one of the film deposited at higher oxygen pressure ($Y|_{t_1}^{0.5}$), although with a much more smeared step in ε' and a broader loss peak in ε''.

The real (ε') and imaginary parts (ε'') of the complex permittivity can be simultaneously fitted with appropriate dielectric dispersion models. Many mathematic models were proposed to interpret the frequency dependence of the ε^* value. After the work of Cole-Cole[23] and Curie-von Schweidler[24, 25], it has been recognized that the observed dielectric response of most solid dielectrics deviates more or less drastically from the classical Debye behaviour. Nowadays it is well established that in highly disordered systems such as amorphous semiconductors or p-n junctions, polymers, biological materials, heavily doped crystals and charge-carrier dominated systems in general, the dielectric response is usually given by a fractional power law in frequency. Such behaviour was denoted as universal dielectric response (UDR) by Jonscher[26, 27].

Among our samples, the dielectric response of $Y|_{t_1}^{0.05}$ and $Y|_{t_2}^{0.05}$, which significantly deviate from the classical Debye behaviour, can be fitted by the UDR model where the complex dielectric constant is given by:

$$\varepsilon^* = \varepsilon_\infty + A(j\omega)^{-(1-n)} \quad (5)$$

where *A* is a temperature dependent parameter, ε_∞ denotes the high frequency value of dielectric constant, ω is the angular frequency and n is a parameter, typically 0.5<n<0.9 for charge-carrier dominated material systems characterized by a dielectric response showing a power law behaviour with the frequency.

The real and imaginary part are given by:

$$\varepsilon' = \varepsilon_\infty + \frac{A}{\varepsilon_0} tan\left(\frac{n\pi}{2}\right) \omega^{-(1-n)} \quad (6)$$

and

$$\varepsilon'' = \frac{\sigma_{DC}}{\varepsilon_0 \omega} + \frac{A}{\varepsilon_0}\omega^{-(1-n)} \quad (7)$$

However, these power-law relations are not able to describe the dielectric behaviour of the $Y|_{t_1}^{0.5}$ film in the entire frequency range, due to the downturn of ε' at intermediate frequencies and the corresponding Debye-like loss peak in ε''. As we will see in the following, this sample is characterized by a 'near Debye' dielectric response in which a loss peak is visible and the high frequency branch follows the power-law with exponent n close to zero (n ≤0.1)[28]. These features highlight the departure from a pure UDR to a more general behaviour, which could be better described by the Cole-Cole equation.

To describe the Debye-type dielectric relaxation, a simple Cole-Cole relaxation equation is generally used, but in the case of $Y|_{t_1}^{0.5}$ sample, the resulting fit (Fig. 5) is not able to reproduce the entire frequency range, because the experimental low frequency dielectric dispersion is not constant. This discrepancy can be attributed to the electrical conductivity that dominates the dielectric response below 1 kHz. Thus, a modified Cole-Cole equation should be used, where the electrical conduction is taken into account as an additional term, as follows[29]:

$$\varepsilon^* = \varepsilon_\infty + \frac{\varepsilon_S - \varepsilon_\infty}{1+(j\omega\tau)^{1-n}} - j\left[\frac{\sigma^*}{\varepsilon_0 \omega^S}\right] \quad (8)$$

where ε_s and ε_∞ denote, respectively, the static and high frequency values of dielectric constant, τ is the dielectric relaxation time and n is a parameter ranging between 0 and 1. In the limit ω→∞, the first two terms gives the same functional form of equation 5, associated to UDR relation, which can be seen as the high-frequency asymptotic form of the Cole-Cole equation[30].

For an ideal Debye relaxation, $n = 0$, while $n > 0$ in the case of a distribution of relaxation times, leading to a broader peak than the simplest Debye case. Thus the n value represents a measure of the deviation from the ideal Debye behaviour. In the conductivity term, enclosed in square bracket in Eq.8, s is a dimensionless exponent (0<s<1) and σ^* is the complex conductivity defined as $\sigma^* = \sigma_{DC} + j\sigma_{sc}$, with σ_{DC} the conductivity due to the free charge carrier (DC conductivity) and σ_{sc} the conductivity component associated to the localized charges (space charges). For an ideal complex conductivity s=1, while s<1 indicates a distribution of carrier polarization mechanism. Working on Eq. 8, the complex permittivity can be decomposed into the real and imaginary part[29]:

$$\varepsilon' = \varepsilon_\infty + \frac{(\varepsilon_S - \varepsilon_\infty)[1+(\omega\tau)^{1-n}sin(n\pi/2)]}{1+2(\omega\tau)^{1-n}sin(n\pi/2)+(\omega\tau)^{2-2n}} + \frac{\sigma_{SC}}{\varepsilon_0 \omega^S} \quad (9)$$

and

$$\varepsilon'' = \frac{(\varepsilon_S - \varepsilon_\infty)(\omega\tau)^{1-n}cos(n\pi/2)}{1+2(\omega\tau)^{1-n}sin(n\pi/2)+(\omega\tau)^{2-2n}} + \frac{\sigma_{DC}}{\varepsilon_0 \omega^S} \quad (10)$$

It is worth noting that the two terms in Eq. 10 are related to different loss mechanisms. Specifically, the first term is associated to the dielectric relaxation due to permanent dipole orientation or other motions that involve localized relaxation, whereas the second term results from long-range migration of mobile charge carriers. The Eq. 9 and 10 indicate that the conductivity may contribute to both the real and the imaginary parts of the permittivity. In particular the space charge conduction, due to the charged defects at the interfaces, contributes to the dielectric permittivity and the DC conduction, due to the free charge carriers, contributes to the dielectric loss.

The fits of the dielectric data of our samples are shown in Fig. 4 (solid lines) and the obtained main fitting parameters are summarized in Table 2. A more detailed figure of the $Y|_{t_3}^{0.05}$ fit is reported in Fig. S2 in the Supporting Information. For films $Y|_{t_1}^{0.5}$ and $Y|_{t_3}^{0.05}$, this modified Cole-Cole equation permits to fit the real part of complex permittivity over the entire frequency range, but it is still not able to catch the details of the high frequency dielectric response of the imaginary part ε'', as shown in Fig. 5 (black curve). The shallow minimum displayed in $\varepsilon''(Y|_{t_1}^{0.5})$ and $\varepsilon''(Y|_{t_3}^{0.05})$ (Fig. 4b) could be ascribed to a superlinear power law (SLPL) conducting regime, as discussed by Lunkenheimer et al. [31, 32] in their dielectric investigations on different disordered materials, such as hexagonal perovskites $La_{1.2}Sr_{2.7}BO_{7.33}$ (B=Ru,Ir).

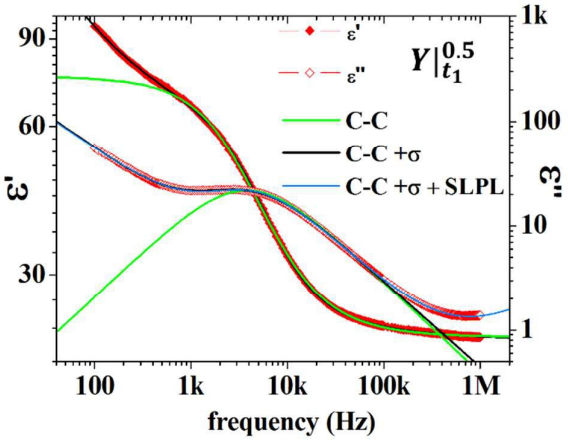

Fig. 5 Best fit of the dielectric response using a Cole-Cole equation and its modified version by adding the conduction contribution and a superlinear power law term at low and high frequencies respectively.

It is important to discuss the values of the exponent *n* (in Table 2), since a relatively higher value of *n* corresponds to a more disordered system. Indeed we found that moving from a near Debye (sample $Y|_{t_1}^{0.5}$) to UDR dielectric response ($Y|_{t_1}^{0.05}$ and $Y|_{t_2}^{0.05}$ samples), the exponent value ranges from 0.07 to 0.78. It should be also observed that by increasing the exponent value, the loss peak disappears and the power-law behaviour becomes dominant. For n=0.58 (sample $Y|_{t_3}^{0.05}$) an intermediate behaviour is observed with barely visible loss peak and clear frequency-dependent relaxation. While the thicker films deposited at 0.05 Pa are characterized by similar values of n (0.76-0.78) and show a similar dielectric response, the thinner film deposited at the same oxygen pressure and the thicker one deposited at 0.5Pa are characterized by very different values of n and dielectric response. These results support a difference in film microstructure, which could be further confirmed by a more detailed structural investigation.

By analyzing the immaginary part of the permittivities (ε"), it is possible to observe that, in the frequency region 100 kHz – 1 MHz, the sample $Y|_{t_1}^{0.5}$ has the lower value of ε", followed by $Y|_{t_3}^{0.05}$, $Y|_{t_1}^{0.05}$ and $Y|_{t_2}^{0.05}$. This trend can be ascribed to a higher oxygen content in the bulk of the film deposited at 0.5Pa with respect to those deposited at 0.05Pa. In addition the lower ε" value for the thinner film can be a consequence of its partial re-oxidation during cool down. The different conductivity between $Y|_{t_3}^{0.05}$ and $Y|_{t_1}^{0.5}$ samples, is highlighted by the different relaxation time extracted from the fitting process (τ=3.69x10^{-5}s and 2.05x10^{-5}s for $Y|_{t_3}^{0.05}$ and $Y|_{t_1}^{0.5}$ respectively), being τ inversely proportional to the conductance of the bulk of the film.

Moreover it is widely accepted[28, 33] that the power-law dielectric relaxation is a typical signature of the disordered matter, in which conduction takes place by hopping as a consequence of charge carriers localization due to disorder arising from amorphous structure, slight deviations from stoichiometry, doping or lattice imperfections. Considering that (i) the samples $Y|_{t_1}^{0.05}$ and $Y|_{t_2}^{0.05}$ show the dielectric features of the UDR behaviour, (ii) they could possess a mixed valence structure of Cu(I)/(II) and Ti(III)/(IV) due to the oxygen-vacancies induced by low P_{O_2} and (iii) they are amorphous in structure, we tentatively assign their dielectric dispersion to the charge-hopping polarization process.

At this point, the last issue to explore regards the understanding of the origin of the permittivity drop and the loss peak at intermediate frequency in $Y|_{t_1}^{0.5}$ and $Y|_{t_3}^{0.05}$. To investigate this feature we performed a capacitance-voltage characterization, in order to figure out if it has an intrinsic or extrinsic nature. From the studies reported in literature on different complex oxides, such as CCTO, it is well known that the low frequency dielectric response could be dominated by extrinsic effects, such as surface barrier layer capacitance (SBLC) or internal barrier layer capacitance (IBLC) that are voltage dependent since they behave as Schottky-type barriers[34-37].

Table 2 Main parameters extracted by fitting both the real and imaginary part of the permittivity of YCTO films with modified Cole-Cole and UDR equations.

sample	Dielectric analysis				
	Cole-Cole/UDR				
	σ_{DC} (10^{-10} S cm^{-1})	σ_{SC} (10^{-10} S cm^{-1})	s	n	τ (10^{-5} s)
$Y|_{t_1}^{0.05}$	1.66			0.76	
$Y|_{t_2}^{0.05}$	169			0.78	
$Y|_{t_3}^{0.05}$	0.41	0.35	0.54	0.58	2.05
$Y|_{t_1}^{0.5}$	2.35	0.90	0.64	0.07	3.69

Capacitance-voltage characterization

Fig. 6 shows the permittivity-frequency ($\varepsilon' - f$) curves of the YCTO capacitors measured by applying an additional DC bias beyond the measuring AC voltage. The dielectric constant remains almost voltage independent in $Y|_{t_1}^{0.05}$and $Y|_{t_2}^{0.05}$ samples, while it decreases with increasing bias voltage in the low frequency range in $Y|_{t_1}^{0.5}$ and $Y|_{t_3}^{0.05}$ samples, most significantly in the first one.

In general, for bulk ceramic materials, the observed responses at low and high frequencies can be attributed to the contributions from electrodes or grain boundaries and bulk respectively. In our case due to the amorphous structure of the YCTO thin films, there are no grain boundaries and only film/electrode interfaces and bulk could contribute to the dielectric relaxations. Therefore, in $Y|_{t_1}^{0.5}$ and $Y|_{t_3}^{0.05}$ samples the low frequency (from 100Hz to 10kHz) dielectric response could be ascribed to top and bottom interfaces, while the high frequency response without evident voltage dependence corresponds to the bulk of the films. This suggest also that $Y|_{t_1}^{0.05}$ and $Y|_{t_2}^{0.05}$ films are characterized by a bulk dominated response in the whole frequency range.

This is further corroborated by the voltage dependence of the percentage capacitance variation ΔC/C (%) as reported in the insets of Fig. 6. For samples $Y|_{t_1}^{0.5}$ and $Y|_{t_3}^{0.05}$, a decrease is observed as expected for a depletion-layer Schottky capacitance:

$$C = \sqrt{\frac{e\varepsilon' N_d}{2(V_d+V)}} \qquad (11)$$

where N_d is the donor concentration and V_d is the diffusion potential.

In samples $Y|_{t_1}^{0.5}$ and $Y|_{t_3}^{0.05}$, the observed decrease in permittivity with increasing frequency (following a Debye-like relaxation) and the voltage dependent capacitance (following the Schottky relation) can be attributed to the Maxwell-Wagner interfacial polarization effect [38] due to the presence of electrical heterogeneous regions in the film. $Y|_{t_1}^{0.5}$ response is also in agreement with a recent report of a Schottky behaviour for ceramic samples prepared in an oxygen atmosphere in contrast to samples prepared in air or vacuum where oxygen vacancies can act as traps[39]. The similar behaviour exhibited by sample $Y|_{t_3}^{0.05}$ can suggest an easier inclusion of oxygen in thinner films. The asymmetry in the curves which is visible in Fig. 6 inset was attributed to dipole anisotropy resulting in an occupation imbalance of trap defects.

The other two samples ($Y|_{t_1}^{0.05}$ and $Y|_{t_2}^{0.05}$), instead, exhibit only a minor increase of the capacitance with the voltage which can be ascribed to a trap charge repositioning process. Thus, non-intrinsic/interface contributions are negligible for them.

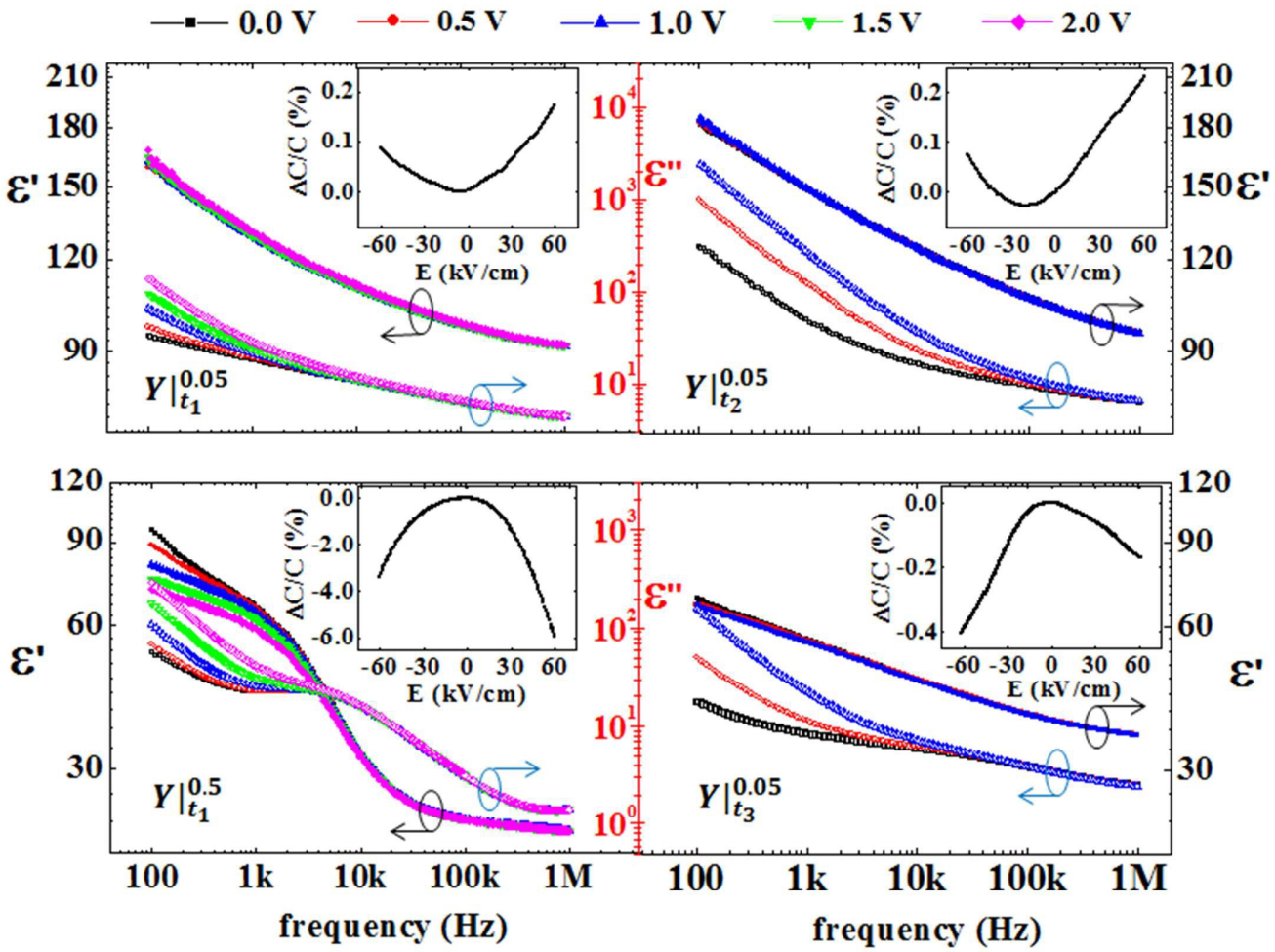

Fig. 6 Capacitance as a function of the frequency at different fixed DC bias values: 0V (black), 0.5V (red), 1V (blue), 1.5V (green) and 2V (magenta), with filled and empty points corresponding to ε' and ε'' respectively. Inset: Percentage variation of the capacitance as a function of the electric field measured at 1 kHz showing a Schottky response for samples $Y|_{t_1}^{0.5}$ and $Y|_{t_3}^{0.05}$ while in the other samples an increase is observed which can be associated to the presence of traps.

Conclusions

In conclusion, we performed the first systematic study of YCTO thin films by varying the oxygen deposition pressure from 0.05 Pa to 0.5 Pa and the thickness from hundreds to tens of nanometers. A very high dielectric constant (around 100) was observed for the thick films deposited at 0.05Pa. This value as well as the frequency dependence of dielectric response was found to vary significantly as a function of the growing parameters. In particular, the films ($Y|_{t_1}^{0.05}$and $Y|_{t_2}^{0.05}$) grown at low oxygen pressure (0.05Pa) exhibit a universal dielectric response along with an almost voltage independent dielectric constant which can be attributed to a charge hopping polarization process due to a mixed valence character of the transition metal ions as a consequence of oxygen vacancies resulting from the low P_{O_2}. On the other hand, increasing the oxygen pressure (0.5Pa) a Maxwell-Wagner behaviour has been observed in $Y|_{t_1}^{0.5}$ film, indicating electrically heterogeneous films, with alternatively dominating bulk and interface contributions depending on the AC frequency. This conclusion is supported by the fits with a modified Cole-Cole equation and the results of voltage dependent studies. The thinner sample deposited at 0.05Pa needs a separate discussion since it also exhibits signatures of interfacial

effects in the frequency and voltage dependence as $Y|_{t_1}^{0.5}$ and contrarily to the thicker samples deposited at the same Po_2 ($Y|_{t_1}^{0.05}$and $Y|_{t_2}^{0.05}$). However, this response can be attributed to a partial oxidation of the film surface during cool down.

Further insight on the physical origin of the dielectric response could be provided by temperature dependent studies of the dielectric response.

As far as applications are concerned, our study demonstrates that YCTO thin films exhibit a high dielectric constant widely tunable by acting on the deposition conditions. In this regard, the thinnest film being characterized by (i) low conductivity in all the frequency range investigated, (ii) a less pronounced loss peak and a relatively high dielectric constant, is very promising as high-k gate oxide.

Acknowledgements

This work was financially supported by the Italian Ministry of Foreign Affairs and the Department of Science and Technology, Government of India through the high-relevance project "Spintronic devices for mass-scale electronics" within the program for scientific and technological co-operation between Italy and India. This work was also financially supported by the MIUR-FIRB Project (prot. RBAP117RWN).

Notes and references

1. D. Choudhury, A. Hazarika, A. Venimadhav, C. Kakarla, K. T. Delaney, P. S. Devi, P. Mondal, R. Nirmala, J. Gopalakrishnan and N. A. Spaldin, *Physical Review B*, 2010, **82**, 134203.
2. K. Singh, N. Kumar, B. Singh, S. Kaushik, N. Gaur, S. Bhattacharya, S. Rayaprol and C. Simon, *Journal of superconductivity and novel magnetism*, 2011, **24**, 1829-1838.
3. D. Choudhury and D. Sarma, *Journal of Vacuum Science & Technology B*, 2014, **32**, 03D118.
4. N. Floros, J. T. Rijssenbeek, A. B. Martinson and K. R. Poeppelmeier, *Solid state sciences*, 2002, **4**, 1495-1498.
5. M. R. Palacín, J. Bassas, J. Rodríguez-Carvajal and P. Gómez-Romero, *Journal of Materials Chemistry*, 1993, **3**, 1171-1177.
6. P. Gómez-Romero, M. Palacín, N. Casañ, A. Fuertes and B. Martínez, *Solid state ionics*, 1993, **63**, 603-608.
7. M. Palacin, J. Bassas, J. Rodriguez-Carvajal, A. Fuertes, N. Casan-Pastor and P. Gomez-Romero, *Materials research bulletin*, 1994, **29**, 973-980.
8. D. Choudhury, A. Venimadhav, C. Kakarla, K. T. Delaney, P. S. Devi, P. Mondal, R. Nirmala, J. Gopalakrishnan, N. A. Spaldin and U. V. Waghmare, *Appl. Phys. Lett.*, 2010, **96**, 162903.
9. W. Yang, M. Mao, X. Liu and X. Chen, *Journal of Applied Physics*, 2010, **107**, 124102.
10. L. Ni and X. M. Chen, *Appl. Phys. Lett.*, 2007, **91**, 122905.
11. L. Ni and X. M. Chen, *Journal of the American Ceramic Society*, 2010, **93**, 184-189.
12. R.-B. Zhang, C.-S. Yang and G.-P. Ding, *Materials Letters*, 2005, **59**, 1741-1744.
13. N. Izyumskaya, Y. Alivov and H. Morkoc, *Critical Reviews in Solid State and Materials Sciences*, 2009, **34**, 89-179.
14. A. Perea, J. Gonzalo, C. Budtz-Jørgensen, G. Epurescu, J. Siegel, C. N. Afonso and J. Garcia-Lopez, *Journal of Applied Physics*, 2008, **104**, 084912.
15. H.-C. Li, W. Si, A. D. West and X. Xi, *Appl. Phys. Lett.*, 1998, **73**, 464-466.
16. L. Sinnamon, R. Bowman and J. Gregg, *Appl. Phys. Lett.*, 2001, **78**, 1724-1726.
17. P. Bao, T. Jackson, X. Wang and M. Lancaster, *Journal of Physics D: Applied Physics*, 2008, **41**, 063001.
18. H. Yang, N. Suvorova, M. Jain, B. Kang, Y. Li, M. Hawley, P. Dowden, R. DePaula, Q. Jia and C. Lu, *Appl. Phys. Lett.*, 2007, **90**, 232909-232909-232903.
19. N. Sama, C. Soyer, D. Remiens, C. Verrue and R. Bouregba, *Sensors and Actuators A: Physical*, 2010, **158**, 99-105.
20. X. Lou and J. Wang, *Journal of Physics: Condensed Matter*, 2010, **22**, 055901.
21. P. Lunkenheimer, R. Fichtl, S. Ebbinghaus and A. Loidl, *Physical review B*, 2004, **70**, 172102.
22. Y. Li, Y. Shen, Z. Hu, F. Yue and J. Chu, *Physics Letters A*, 2009, **373**, 2389-2392.
23. K. S. Cole and R. H. Cole, *The Journal of Chemical Physics*, 1941, **9**, 341-351.
24. E. R. V. Schweidler, *Annalen der Physik*, 1907, **329**, 711-770.
25. J. Curie, *Recherches sur le pouvoir inducteur spécifique et sur la conductibilité des corps cristallisés, par M. Jacques Curie*, " la Lumière électrique, 1888.
26. A. K. Jonscher, *Nature*, 1977, **267**, 673-679.
27. A. K. Jonscher, *Journal of Physics D-Applied Physics*, 1999, **32**, R57-R70.
28. A. K. Jonscher, *Ieee Transactions on Electrical Insulation*, 1992, **27**, 407-423.
29. P. Thongbai, S. Tangwancharoen, T. Yamwong and S. Maensiri, *Journal of Physics: Condensed Matter*, 2008, **20**, 395227.
30. A. Jonscher, *Chelsea Dielectric, London*, 1983.
31. P. Lunkenheimer, T. Götzfried, R. Fichtl, S. Weber, T. Rudolf, A. Loidl, A. Reller and S. Ebbinghaus, *Journal of Solid State Chemistry*, 2006, **179**, 3965-3973.
32. P. Lunkenheimer and A. Loidl, *Physical review letters*, 2003, **91**, 207601.
33. P. Lunkenheimer, S. Krohns, S. Riegg, S. G. Ebbinghaus, A. Reller and A. Loidl, *Eur. Phys. J. Spec. Top.*, 2009, **180**, 61-89.
34. T. B. Adams, D. C. Sinclair and A. R. West, *Physical Review B*, 2006, **73**, 094124.
35. T. B. Adams, D. C. Sinclair and A. R. West, *Advanced Materials*, 2002, **14**, 1321-1323.
36. P. Lunkenheimer, V. Bobnar, A. Pronin, A. Ritus, A. Volkov and A. Loidl, *Physical Review B*, 2002, **66**, 052105.
37. D. Gutiérrez, M. Foerster, I. Fina, J. Fontcuberta, D. Fritsch and C. Ederer, *Physical Review B*, 2012, **86**, 125309.
38. W. Li and R. W. Schwartz, *Physical Review B*, 2007, **75**, 012104.
39. X. J. Luo, C. P. Yang, X. P. Song, S. L. Tang, H. B. Xiao and K. H. O. Bärner, *Journal of the American Ceramic Society*, 2013, **96**, 253-258.